From airborne to effective-medium spectral IP mineral exploration: a case study in Saudi Arabia

Michael S. Zhdanov, TechnoImaging and the University of Utah; Fouzan Alfouzan, King Abdulaziz City for Science and Technology; Leif H. Cox, TechnoImaging; Abdulrahman Alotaibi, King Abdulaziz City for Science and Technology*

SUMMARY

The Saudi Arabian Glass Earth (Pilot) project is a geophysical exploration project to explore the upper crust of the Kingdom for minerals, groundwater, and geothermal resources as well as strictly academic investigations. The project began with over 8000 km^2 of green fields area. Airborne geophysics including EM, magnetics, and gravity were used to develop several high priority targets for ground follow-up. Based on the results of airborne survey, a spectral induced polarization (SIP) survey was completed over one of the prospective targets. The field SIP data were inverted using the GEMTIP model in conjunction with an integral equation-based modeling and inversion code. This code can replicate all inductive coupling and EM effects, which removes one large barrier to inversion of large bandwidth spectral IP data. The results of this inversion were interpreted, and several drill holes sited. The drill holes intersected significant mineralization which is currently being further investigated. The project can be considered a technical success, validating the methods and effective-medium inversion technique used for the project.

INTRODUCTION

The Saudi Arabian Glass Earth project is a multiyear Earth observation project designed to explore for resources in the relatively unexplored regions of Saudi Arabia. The initial stage of the project involved the acquisition, processing, and interpretation of airborne electromagnetic, gravity, and magnetic geophysical data over an 8000 square kilometer area (Zhdanov et al., 2018a). The project helped to identify a dozen potential mining targets. A follow-up ground spectral induced polarization (SIP) survey was conducted to further investigate one of the identified anomalies. The SIP data were collected by Dias Geophysical with their distributed array system.

Distributed array systems can collect 10,000s to millions of data points which contain information about the 3D distribution of time dependent or frequency dependent complex conductivity of the medium. This information can be translated into knowledge about mineralization which goes well beyond that contained in conventional conductivity. In fact, it may be possible to discriminate economic and non-economic mineralization from the surface using this technique (Zonge and Wynn, 1975; Pelton et al., 1975, 1978a, b).

However, the major road blocks to a widespread use of this technology are a lack of a model which describes and properly characterizes the complex conductivity response of different media (microscopic effects), and a lack of suitable software and methods to process and interpret large volumes of the SIP data with a technique which is rigorous enough to honor all the macroscopic physical effects. We address these two issues with our new inversion code which uses the generalized effective medium theory of induced polarization (GEMTIP), introduced by Zhdanov (2008a,b, 2018b). The inversion code also honors all the macroscopic physics of electromagnetic field which is required for modeling.

In this paper, we apply the advanced modeling and inversion methods to the spectral IP data collected in Saudi Arabia during the Glass Earth Pilot Project. We use an efficient integral equation forward modeling scheme for the forward modeling. We solve for the four dominate GEMTIP parameters for each voxel in the inversion domain. The re-weighted conjugate gradient method is used to optimize the search for the minimum of the objective functional.

Based on the results of the inversion, we developed two targets in a green fields area of Saudi Arabia. Both targets were drilled, and mineralization was confirmed in both drill holes. This is a significant technical success.

METHODS

GEMTIP resistivity relaxation model

In a general case, the effective conductivity of rocks is not necessarily a constant and real number, but is complex and may vary with frequency. A general approach to constructing the resistivity relaxation model is based on the rock physics and description of the medium as a composite heterogeneous multiphase formation (Zhdanov, 2008a).

In the paper by Burtman et al. (2016), we introduced for simplicity, the frequency dependent complex resistivity for a two-phase model with elliptical inclusions, described by the following formula:

$$\rho_e = \rho_0 \left\{ 1 + \frac{f}{3} \sum_{\alpha=x,y,z} \frac{1}{\gamma_\alpha} \left[1 - \frac{1}{1 + s_\alpha (i\omega\tau)^{C_1}} \right] \right\}^{-1}, \quad (1)$$

where ρ_0 is the DC resistivity (Ohm-m); ω is the angular frequency (rad/sec), τ is the time parameter; and C is the relaxation parameter. The coefficients γ_α and $s_\alpha (\alpha = x, y, z)$ are the structural coefficients defined by geometrical characteristics of the ellipsoidal inclusions used to approximate the grains.

Regularized integral equation inversion

There are several advantages of using the IE method in IP data inversion in comparison with the more traditional finite-difference (FD) approach. First, IE forward modeling requires the calculation of the Green's tensors for the background conductivity model. These tensors can be precomputed only once and saved for multiple use on every iteration of an inversion, which speeds up the computation of the predicted data (Gribenko

10.1190/segam2019-3213407.1

and Zhdanov, 2007). IE forward modeling and inversion require the discretization of the domain of inversion only, while in the framework of the FD method one must discretize the entire modeling domain, which includes not only the area of investigation but an additional domain surrounding this area (including the areas in the air as well). For this reason, the IE inversion method requires just one forward modeling on every iteration step, which speeds up the computations and results in a relatively fast but rigorous inversion method.

The inversion is based on minimization of the Tikhonov parametric functional, $P^{\alpha}(\sigma)$, with the corresponding stabilizer $S(\sigma)$ (Tikhonov and Arsenin, 1977):

$$P^{\alpha}(\sigma) = \|\mathbf{W}_d(A(\sigma) - \mathbf{d}\|^2_{L_2} + \alpha S(\sigma), \qquad (2)$$

where $\mathbf{W}_d$ is the data weighting matrix, and α is a regularization parameter used to balance the misfit and stabilizer terms in equation (2). We use the regularized conjugate gradient method to find the solution of the inverse problem (Zhdanov, 2002).

Calculation of the Fréchet derivatives with respect to the GEMTIP model parameters

In the current project, we consider the GEMTIP model describing a two-phase composite medium. This GEMTIP model is characterized by four parameters (conductivity of the host medium, σ_0; fraction volume f; time constant, τ; and relaxation coefficient, C). Therefore, the Fréchet derivatives with respect to each GEMTIP parameter are required to invert the IP data.

We find the sensitivities of each model cell to the data by using the extended Born approximation for conductivity. The Fréchet derivative of each GEMTIP model parameter is then found by using partial derivatives of the conductivity sensitivity and the chain rule. All modeling is done in the frequency domain. In order to compute the Fréchet derivatives in the time domain, we use a cosine transform of the quadrature part of the spectrum to obtain a step response.

Geologic background of study area

The original regional study area covered by the airborne EM, magnetics, and gravity comprises three distinct geologic regimes. In the far west of the study area the Precambrian Arabian shield forms mountains up to nearly 1 km above the surrounding land. In the central part of the survey are Cenozoic volcanic rocks (harrats) that average several hundred meters in thickness and with a maximum thickness of around 400-700 m. These are underlain by the Arabian shield. Approximately the eastern 1/3 of the survey area covers Arabian shield with sediment filled basins and mountains of locally high relief (100s m). The Quaternary sediments in the areas are predominately wadi alluvium, Aeolian sand and sand dunes, and terraced, slightly consolidated alluvium of old wadi deposits.

The geologic maps of the area show several mineral occurrences in the Arabian shield area in the eastern 1/3 of the survey area. Many of these were historic mines of archaeological interest, but little modern mineral extraction has occurred in the area. Of special note is the Mahd Ad Dahab mine, which is located just southeast of the study area, and is the largest mine in Saudi Arabia.

Geophysical background

From the airborne data, several large-scale regional features were discovered (Zhdanov et al., 2018a). Many small-scale anomalies (100s meters areal extent) were also seen based on the Glass Earth models of the physical properties of the subsurface. Note that, most of these anomalies are located on or very close to the large regional features that have been identified. The fact that both copper and gold mineralization is known in the surrounding area is very encouraging.

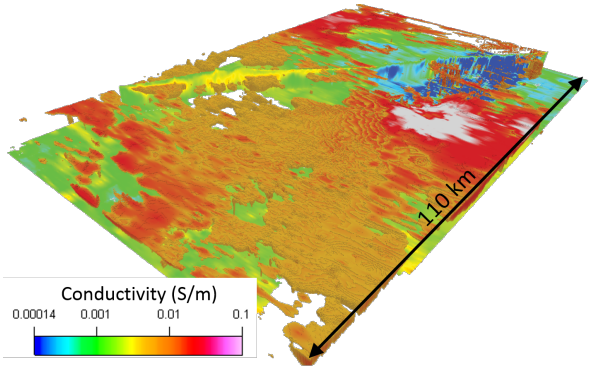

Figure 1: Perspective view of the regional conductivity model. A horizontal slice and a vertical slice are shown along with voxels which have less than 100 Ohm-m resistivity

The targets that we choose to follow-up are all in exposed shield, all are conductive anomalies, and many have associated magnetic signatures. We made one of the selected targets because the shape of the target suggested alteration or mineralization, and not saline groundwater or overburden. Both are likely very common conductive bodies in this region. Also, there are magnetics associated with the conductive anomaly, which is another strong sign for mineralization. The conductivity and magnetics associated with this deposit, as obtained from the airborne data, are shown in Figure 2.

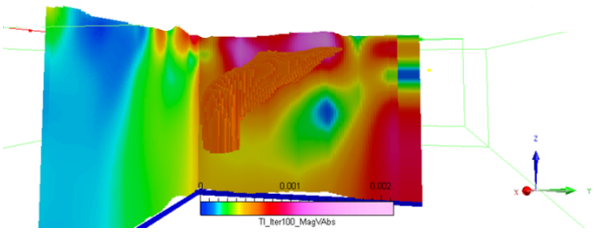

Figure 2: Perspective view of the target. The cut-away view is the conductive body (> 0.1 S/m) and the slices show the magnetic vector amplitude. There is a clear correlation between the two.

From these images, it appears the body exhibits both a magnetic response and an elevated electrical conductivity. The body is cigar shaped dipping steeply to the south-southeast.

10.1190/segam2019-3213407.1

It is near a large regional structure mapped with both the gravity and the electromagnetic techniques. There is conductive overburden can be seen near the target, but the body is clearly hosted in the resistive bedrock.

The outstanding question is 'does this body contain mineralization?'. This cannot be wholly established by geophysics alone but determining if the body has an induced polarization response goes a long way towards increasing the certainty of this conductivity anomaly is due to mineralization, and possibly and economic mineral deposit. The spectral induced polarization method is a great compliment to airborne EM. Being a resistive method, it does an excellent job of imaging targets of moderate resistivity or conductivity. It also can differentiate between disseminated sulfides, massive sulfides, and clays or groundwater of similar conductivity.

FIELD DATA

Ground induced polarization data collection

Dias Geophysical collected the spectral IP data with their 3D distributed array system (Rudd and Chubak, 2017). The ground IP survey was designed with five three-kilometer-long lines oriented such that they were perpendicular to dominate geologic strike in the area. The survey used 100 m grounded dipoles as sources and receivers to best collected spectral IP data. The line spacing was 350 m. These lines are shown in Figure 3 overlain on a shaded terrain image. The SIP data are collected as a time series of voltage with each current injection. The majority of the current injection dipoles used a 50% duty cycle 8s square wave. Each current injection point undergoes several minutes of current injection with the waveform being recorded at the injection points. The voltage at the receivers is recorded continuously throughout their entire deployment.

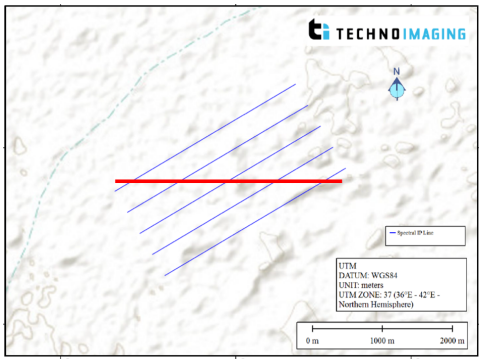

Figure 3: Location of spectral IP lines overlain on a DTM. Each line is approximately 3 km long, and has a line spacing of 350 m. The red line shows the location of the cross-section shown in Figures 5 and 6

INVERSION RESULTS AND INTERPRETATION

The inversion was run according to the description above. The data weights were assigned to be the inverse of the estimated error in each data point. The inversion converged from a normalized χ^2 of around 3 to 1.1.

Figure 4 shows an example of observed and predicted data from line 2. The black dots show measurement points on the pseudo-section. The observed and predicted data match well and are within the estimated error level. This is also demonstrated by the final normalized χ^2 of 1.1. A perfect fit would theoretically have a value of 1.0.

The inversion used almost 3000 unique observation stations, each containing 16 time channels. This gives a total of 48,000 data points. The model was discretized into cells 50 m x 350 m horizontally and varying from 17 to 114 m thick with depth. This gives overs 5,000 model cells and 21,440 unknowns to be solved for when the GEMTIP parameters are considered.

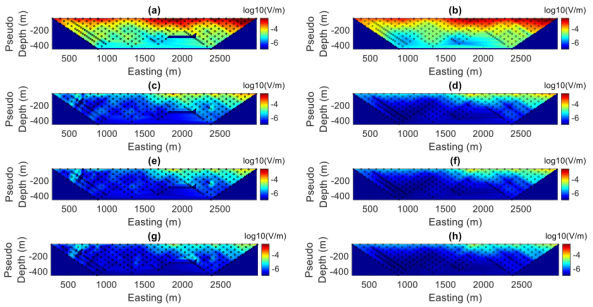

Figure 4: Observed and predicted data from line 2 in pseudo-section form. This is the second line from the south, as shown in Figure 3. The left panels are the observed data, while the right panels are the predicted data. The black dots are the observation points. From top to bottom the panels are Vp (on-time data), and Vs at 85 ms, 340 ms, and 1045 ms. A few spurious noisy data points are shown in the observed data and have been rejected by the inversion algorithm.

Figures 5 and 6 shows east-west cross sections of the recovered conductivity and chargeability along the location shown in Figure 3. A few features are apparent from these figures. First, there is pervasive conductive overburden in this area. This is to be expected in this highly weathered environment. The exceptions are some of the bedrock hills, as demonstrated in the center of the near surface of Figure 5. Most areas below this conductive overburden are resistive, but there are notable exceptions, such as the western third of Figure 5 which shows a dipping conductor.

Regarding the chargeability, the near-surface resistive material also shows the largest chargeability. There is a strong chargeability anomaly shown in the inversion results near the center of Figure 6, which is in the range of 0.1 to 0.2 V/V.

VALIDATION

Based on the comprehensive geophysical information from all ground and airborne data, three targets were identified for drilling. The drill holes were listed in order of priority from drill hole 1

10.1190/segam2019-3213407.1

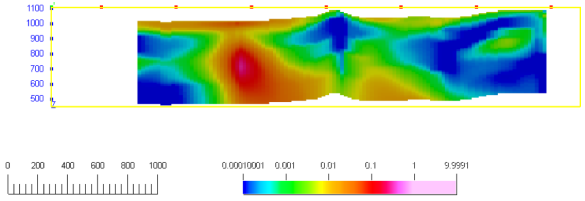

Figure 5: East-west cross-section from the location shown in Figure 3. The vertical axis is depth, and the scale is shown in the lower left (meters). The color bar shows the conductivity in S/m.

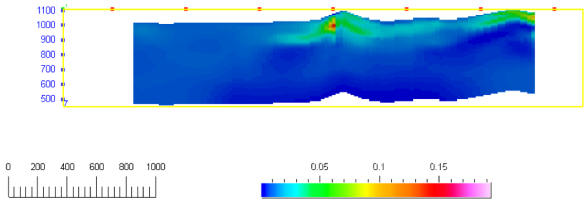

Figure 6: East-west cross-section from the location shown in Figure 3. The vertical axis is depth, and the scale is shown in the lower left (meters). The color bar shows the chargeability in V/V.

to 3. The boreholes were planned to sample different geophysical signatures, such as chargeable and resistive, or conductive.

Drilling results

Borehole 1 was not drilled due to ground conditions. Borehole 2 targets a well defined conductive anomaly and passed through a chargeability anomaly (Figures 7 and 8). Drill hole #2 was logged and the results are shown overlain on the figures.

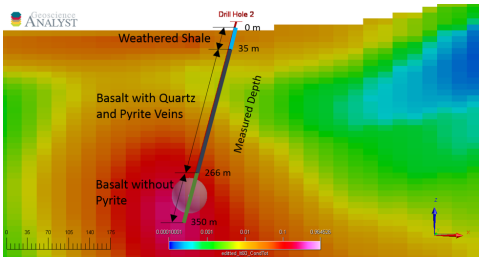

Figure 7: The path for drill hole 1 shown overlain on a vertical chargeability section. The perspective is looking north. A distance scale is shown in the lower left of the image (meters).

The uppermost lithology is a weathered shale, which is moderately conductive and not chargeable. The basalt with quartz is lower conductivity (due to the pyrite) and weakly chargeable (due to the pyrite). Below this is basalt with little pyrite. This account for its lack of chargeability. The deep conductivity high is currently unexplained. The basalt is moderately weathered which would explain an elevated conductivity, but possible there is more alteration or sulfides which are being imaged and were not intersected.

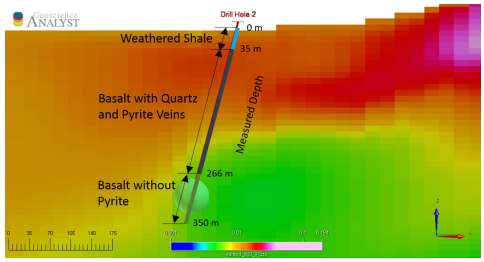

Figure 8: The path for drill hole 1 shown overlain on a vertical conductivity section. The perspective is looking north. A distance scale is shown in the lower left of the image (meters).

The drilling results of targets #2 and #3 show quartz veins filled with the minerals, like pyrrhotite, pyrite, and chalcopyrite, with the presence of gold and silver. This points to a possible epithermal gold and silver vein type deposit. This is further encouraged by the proximity to the Mahd Ahd Dahab and Jabal Sayid deposits, aka the "Cradle of the Gold".

CONCLUSIONS

We have developed a novel method of 3D inversion of spectral IP data based on the GEMTIP conductivity relaxation model. The developed method considers the nonlinear nature of both the electromagnetic induction and the IP phenomena and inverts the EM data to the parameters of the GEMTIP model. The method was validated by the field data inversions of the time domain IP data for the GEMTIP model parameters.

The Glass Earth project has followed an exploration workflow from country wide selection through drill hole targeting and discovery of blind mineralization by using the inversion method detailed in this paper. While the discovery is fortuitous, it would not have happened without the techniques of modern geophysics. There is no surface expression of this mineralization. The 300 m drill hole was sited in an original area of nearly 8000 km^2. Drilling results of targets #2 and #3 show quartz veins filled with the minerals, like pyrrhotite, pyrite, and chalcopyrite, with the presence of gold and silver type of mineralization in our survey area is similar to an epithermal, low-sulfidation, polymetallic type deposit of Mahd Ahd Dahab Mine.

ACKNOWLEDGEMENTS

The authors acknowledge the support of the University of Utah Consortium for Electromagnetic Modeling and Inversion (CEMI). We are thankful to King Abdulaziz City for Science and Technology and TechnoImaging for providing the geophysical data, and permission to publish the results. Special thanks are extended to DIAS for collecting good quality SIP data.

10.1190/segam2019-3213407.1

REFERENCES

Burtman, V., M. Zhdanov, W. Lin, and M. Endo, 2016, Complex resistivity of mineral rocks in the context of the generalized effective-medium theory of the IP effect: 86th Annual International Meeting, SEG, Expanded Abstracts, 2238–2242, doi: https://doi.org/10.1190/segam2016-13848294.1.

Gribenko, A., and M. S. Zhdanov, 2007, Rigorous 3D inversion of marine CSEM data based on the integral equation method: Geophysics, **72**, no. 2, WA73–WA84, doi: https://doi.org/10.1190/1.2435712.

Pelton, W. H., L. Rijo, and C. M. Swift, Jr., 1978a, Inversion of two-dimensional resistivity and induced-Polarization data: Geophysics, **43**, 788–803, doi: https://doi.org/10.1190/1.1440854.

Pelton, W. H., B. D. Smith, and W. R. Sill, 1975, Inversion of complex resistivity and dielectric data: Geophysics, **40**, 153.

Pelton, W. H., S. H. Ward, P. G. Hallof, W. R. Sill, and P. H. Nelson, 1978b, Mineral discrimination and removal of inductive coupling with multi-frequency IP: Geophysics, **43**, 547–565.

Rudd, J., and G. Chubak, 2017, The Facility of a Fully-Distributed DCIP System with CVR: 15th SAGA Biennial Conference and Exhibition.

Tikhonov, A. N., and V. Y. Arsenin, 1977, Solutions of ill-posed problems: Wiley.

Xu, Z., and M. S. Zhdanov, 2015, Three-dimensional Cole-Cole model inversion of induced polarization data based on regularized conjugate gradient method: IEEE Geoscience and Remote Sensing Letters, **12**, 2311–2315, doi: https://doi.org/10.1109/LGRS.2015.2474744.

Yoshioka, K., and M. S. Zhdanov, 2005, Three-dimensional nonlinear regularized inversion of the induced polarization data based on the Cole–Cole model: Physics of the Earth and Planetary Interiors, **150**, 29–43, doi: https://doi.org/10.1016/j.pepi.2004.08.034.

Zhdanov, M. S., 2002, Geophysical inverse theory and regularization problems: Elsevier.

Zhdanov, M. S., 2008a, Generalized effective-medium theory of induced polarization: Geophysics, **73**, no. 5, F197–F211, doi: https://doi.org/10.1190/1.2973462.

Zhdanov, M. S., 2009, Geophysical electromagnetic theory and methods: Elsevier, 848.

Zhdanov, M. S., 2015, Inverse theory and applications in geophysics: Elsevier, 704.

Zhdanov, M. S., F. A. Alfouzan, L. Cox, A. Alotaibi, M. Alyousif, D. Sunwall, and M. Endo, 2018a, Large-Scale 3D Modeling and Inversion of Multiphysics Airborne Geophysical Data: A Case Study from the Arabian Shield, Saudi Arabia: Minerals, **8**, 271, doi: https://doi.org/10.3390/min8070271.

Zhdanov, M. S., V. Burtman, M. Endo, and W. Lin, 2018b, Complex resistivity of mineral rocks in the context of the generalised effective medium theory of the induced polarization effect: Geophysical Prospecting, **66**, 798–817, doi: https://doi.org/10.1111/1365-2478.12581.

Zhdanov, M. S., M. Endo, L. H. Cox, and D. A. Sunwall, 2018c, Effective-medium inversion of induced polarization data for mineral exploration and mineral discrimination: Case study for the copper deposit in Mongolia: Minerals, **8**, 28, doi: https://doi.org/10.3390/min8010028.

Zonge, K. L., and J. C. Wynn, 1975, Recent advances and applications in complex resistivity measurements: Geophysics, **40**, 851–864, doi: https://doi.org/10.1190/1.1440572.